MERCK

catch the SUN

Product Category list:

- Organic Photovoltaic (OPV) Donors and Acceptors
- Dye-Sensitized Solar Cell Materials
- Perovskite Materials

Visit us at:
SigmaAldrich.com/organic-electronics

MK_AD9792EN 43729 08/2022

The Life Science business of Merck operates as MilliporeSigma in the U.S. and Canada.

Sigma-Aldrich®
Lab & Production Materials

ADVANCED ENERGY MATERIALS
www.advenergymat.de

Impacts of the Lattice Strain on Perovskite Light-Emitting Diodes

Heyong Wang, Zhan Chen, Fuyu Tian, Guanhaojie Zheng, Hongguang Wang, Tiankai Zhang, Jiajun Qin, Xingyu Gao, Peter A. van Aken, Lijun Zhang, Xiao-Ke Liu, and Feng Gao**

The development of perovskite light-emitting diodes (PeLEDs) with both high efficiency and excellent stability remains challenging. Herein, a strong correlation between the lattice strain in perovskite films and the stability of resulting PeLEDs is revealed. Based on high-efficiency PeLEDs, the device lifetime is optimized by rationally tailoring the lattice strain in perovskite films. A PeLED with a high peak external quantum efficiency of 18.2% and a long lifetime of 151 h (T_{70}, under a current density of 20 mA cm^{-2}) is realized with a minimized lattice strain in the perovskite film. In addition, an increase in the lattice strain is found during the long-time device stability test, indicating that the degradation of the local perovskite lattice structure could be one of the degradation mechanisms for long-term stable PeLEDs.

H. Wang, Z. Chen, T. Zhang, J. Qin, X.-K. Liu, F. Gao
Department of Physics, Chemistry, and Biology (IFM)
Linköping University
Linköping 58183, Sweden
E-mail: xiaoke.liu@liu.se; feng.gao@liu.se

F. Tian, L. Zhang
State Key Laboratory of Integrated Optoelectronics
Key Laboratory of Automobile Materials of MOE
College of Materials Science and Engineering
Jilin Provincial International Cooperation Key Laboratory of High-Efficiency Clean Energy Materials
Jilin University
Changchun 130012, China

G. Zheng, X. Gao
Shanghai Synchrotron Radiation Facility (SSRF)
Zhangjiang Lab
Shanghai Advanced Research Institute
Chinese Academy of Sciences
Shanghai 201204, China

X. Gao
University of Chinese Academy of Sciences
Beijing 100049, China

H. Wang, P. A. van Aken
Max Planck Institute for Solid State Research
70569 Stuttgart, Germany

The ORCID identification number(s) for the author(s) of this article can be found under https://doi.org/10.1002/aenm.202202185.

DOI: 10.1002/aenm.202202185

1. Introduction

Lead halide perovskites exhibit excellent optoelectronic properties and low-temperature fabrication processes, promising a new generation of low-cost and high-performance light-emitting diodes (LEDs) technology.[1] Over the past several years, extensive efforts have been devoted to achieving high-efficiency perovskite LEDs (PeLEDs),[2] resulting in significant breakthroughs in external quantum efficiencies (EQEs).

A big challenge with the further development of PeLEDs is stability. Recently, several factors affecting the stability of PeLEDs have been demonstrated, mainly including ion migration, thermal instability, and interfacial instability.[3] While different strategies have been employed to address these issues,[4] the lifetimes of high-efficiency PeLEDs are still moderate and fundamental questions on the device stability remain to be further investigated.

Among others, it is unclear how the lattice strain affects the stability of PeLEDs. Lattice strain has been theoretically and experimentally demonstrated in perovskite films. Extensive investigations have demonstrated significant impacts of the strain on perovskite photovoltaic stability and efficiency.[5] However, the situation may be complicated in the state-of-the-art PeLEDs, where largely excess organic salts and/or additives are usually used.[6] On the one hand, these extra salts and additives might passivate the electronic traps in perovskite films for achieving high EQEs in PeLEDs.[2b] On the other hand, they can also affect the crystallization processes of perovskite films,[7] resulting in significantly different perovskite films compared with those in the photovoltaic cases.

Herein, we systematically investigate the impacts of the lattice strain on the stability and efficiency of PeLEDs. For mixed-cation perovskite films with excess formamidinium iodide (FAI), we notice negligible relation between the lattice strain in the perovskite films and the peak efficiency of PeLEDs, yet find a strong correlation between the lattice strain and the device stability. By rationally controlling the amount of Cs^+ cation in perovskite precursors, we achieve a minimum lattice strain in the perovskite film, which consequently results in a significantly improved device lifetime to 151 h (T_{70}, the time taken for the radiance to drop to 70% of its maximum value, measured at a constant current density of 20 mA cm^{-2}). Additionally, we

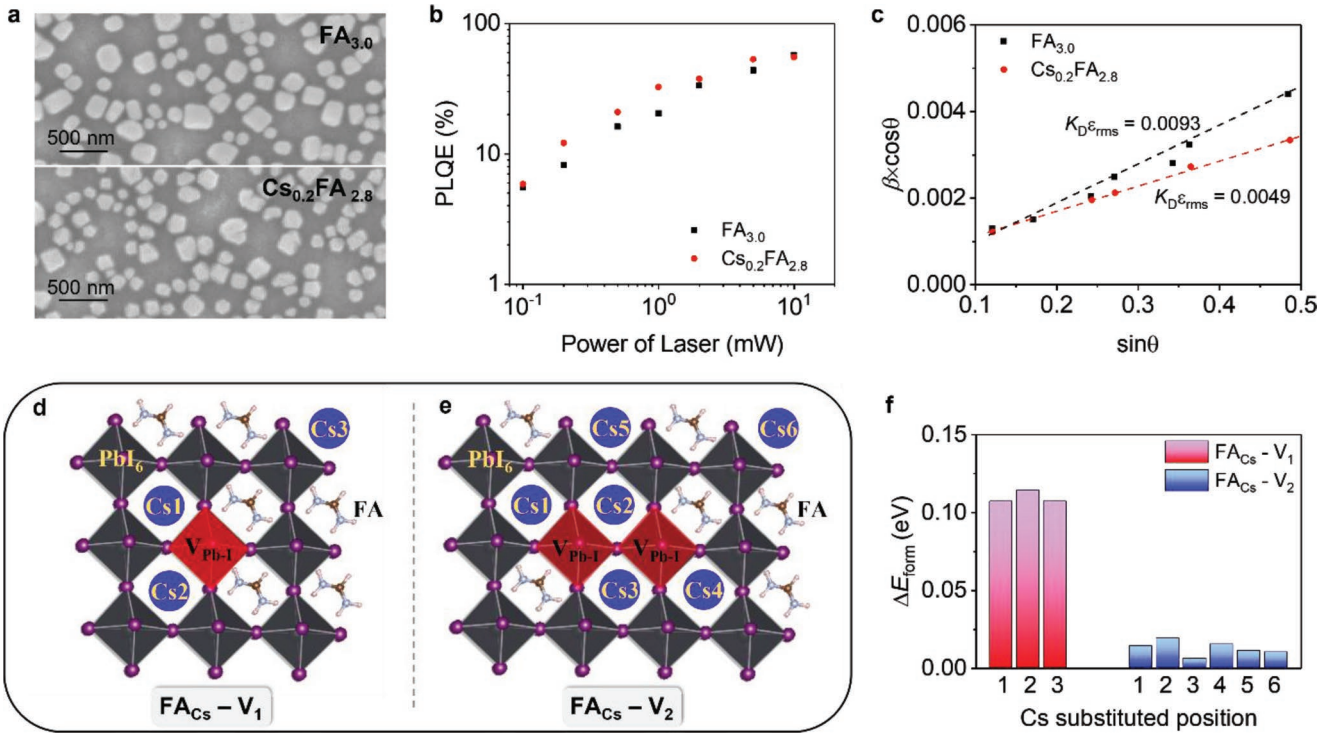

Figure 1. Characteristics of perovskite films. a) SEM images, b) power-dependent PLQEs, and c) Williamson–Hall plots of $FA_{3.0}$ and $Cs_{0.2}FA_{2.8}$ perovskite films. Schematic of the possible positions of one Cs substitution in the presence of d) one [PbI_x] vacancy defect and e) two [PbI_x] vacancy defects. f) The difference in formation energy (ΔE_{form}) between one Cs-substituted $FAPbI_3$ defective structure and a $FAPbI_3$ defective structure.

observe an increase in the lattice strain after a long-time stability test, indicating that the degradation of the local perovskite lattice structure could be a degradation mechanism for the long-term operation of PeLEDs. Our work provides useful guidelines in material design for both high-efficiency and stable PeLEDs as well as a new understanding of degradation mechanisms in PeLEDs with long-term stability.

2. Results and Discussion

2.1. Reducing the Lattice Strain to Enhance the Stability of PeLEDs

The $FAPbI_3$ and (Cs/FA)PbI_3 perovskite films in this study are prepared following our previous method; a molecule (4,4′-diaminodiphenyl sulfone, DDS) is employed to modify the crystallization process of perovskite films for achieving high-quality perovskite crystals.[7] The molar ratio in perovskite precursors of FAI:PbI_2:DDS is 3:1:1 for the $FAPbI_3$ film (denoted as $FA_{3.0}$), while that in (Cs/FA)PbI_3 perovskite precursors of CsI:FAI:PbI_2:DDS is 0.2:2.8:1:1 (denoted as $Cs_{0.2}FA_{2.8}$).

The two perovskite films consist of phase-pure and high-quality isolated perovskite crystals. **Figure 1**a shows top-view scanning electron microscope (SEM) images of the perovskite films, both of which consist of isolated perovskite grains with average sizes of 206 nm (for the $FA_{3.0}$ film) and 180 nm (for the $Cs_{0.2}FA_{2.8}$ film). Figure S1, Supporting Information shows out-of-plane 2θ XRD patterns of the perovskite films. All diffraction peaks can be assigned to lattice planes of their cubic phases,[8] indicating phase-pure perovskites in both perovskite films. Scanning transmission electron microscopy (STEM) and electron energy-loss spectroscopy (EELS) results in Figure S2 show the cross-sectional structure of the $Cs_{0.2}FA_{2.8}$ perovskite film-based LED and the distribution of constituent elements. High-resolution STEM images demonstrate a good crystalline quality of the $Cs_{0.2}FA_{2.8}$ perovskite film, which is similar to our previous results of the $FAPbI_3$ perovskite film[7] In addition, compared with that of the $FA_{3.0}$ film, the diffraction peak of the (001) lattice plane at around 14° of $Cs_{0.2}FA_{2.8}$ film shifts to a larger angle (Figure S1, Supporting Information), in agreement with reduced lattice parameters by alloying small-sized Cs^+ cations. Besides, as shown in Figure S3, Supporting Information, the grazing incidence wide-angle X-ray scattering (GIWAXS) images of both perovskite films demonstrate highly preferential crystallographic orientation. For each GIWAXS pattern, the diffraction peaks of the (001) lattice plane at round q = 10 nm^{-1} are identical at various ψ values, indicating no residual strains in both perovskite films. Furthermore, as shown in Figure 1b, the two perovskite films show similar photoluminescence quantum efficiencies (PLQEs) at various excitation powers, implying similar trap densities in these two perovskite films. The space charge limited current (SCLC) results of the $FA_{3.0}$ and $Cs_{0.2}FA_{2.8}$ -based single-electron devices (Figure S4 and Note S1, Supporting Information) show the same trap density of 2.69×10^{16} cm^{-3}. As such, these two perovskite films demonstrate similar morphologies, crystallinity, and trap densities.

We then investigate the lattice strain in these two perovskite films by analyzing the out-of-plane 2θ XRD data based on

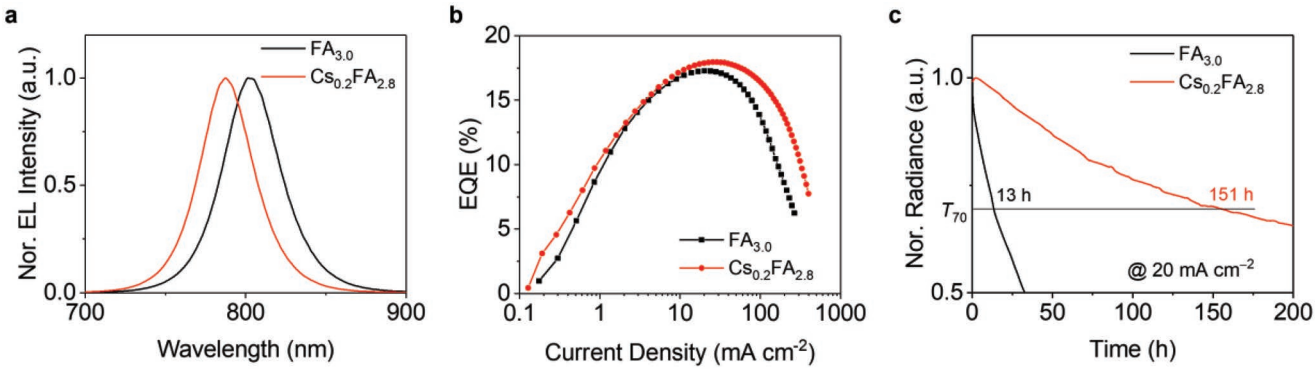

Figure 2. Characteristics of PeLEDs. a) Normalized EL spectra, b) EQE-current density curves, and c) operational stability of $FA_{3.0}$ and $Cs_{0.2}FA_{2.8}$ based PeLEDs.

Williamson–Hall (W–H) plot method,[5a] and demonstrate that the incorporation of Cs^+ cations decreases the lattice strain. The slope ($K_D\varepsilon_{rms}$, where K_D is a constant and ε_{rms} is the average lattice strain) in a W–H plot qualitatively represents the degree of average lattice strain in a film (Note S2, Supporting Information). As shown in Figure 1c, the $FA_{3.0}$ film shows a $K_D\varepsilon_{rms}$ value of 0.0093, which is close to double that of the $Cs_{0.2}FA_{2.8}$ film ($K_D\varepsilon_{rms}$ = 0.0049). This means that the lattice strain in the $FA_{3.0}$ film is larger than that of the $Cs_{0.2}FA_{2.8}$ film. This could be explained by the Goldschmidt tolerance factor. As shown in Figure S5, Supporting Information, in the A-site cation-rich case, a cumulative effect of lattice expansion caused by large-sized FA^+ cations could lead to the formation of local [PbI_x] vacancy defects (x ranges from 0 to 6), resulting in the formation of lattice strain. The Pb vacancy defect is believed to be a shallow defect[9] which does not result in strong non-radiative recombination. This explains the similar PLQEs of $FA_{3.0}$ and $Cs_{0.2}FA_{2.8}$ perovskite films. Mixing small-sized Cs^+ cations can tune the Goldschmidt tolerance factor and suppress the formation of lattice strain. The calculated formation energies of perovskites containing one and two [PbI_x] vacancy defects (Figure 1d–f and Note S3, Supporting Information) also indicate that the substitution of small-sized Cs^+ cations for large-sized FA^+ cations suppresses the formation of lattice strain, in line with the experimental result.

We fabricate PeLEDs based on these two perovskite films. Figure S6, Supporting Information shows the device structure and characteristics of the PeLEDs. STEM images (Figure S6b, Supporting Information) of the cross-section of PeLEDs demonstrate that the two perovskite emissive layers have similar thicknesses of around 60 nm. Compared with the electroluminescent (EL) peak (802 nm) of the $FA_{3.0}$ based PeLED, the EL peak of $Cs_{0.2}FA_{2.8}$ based PeLED blue shifts to 787 nm (**Figure 2**a), in line with modified crystal structures of perovskites by mixing Cs/FA cations. As shown in Figure 2b, the $Cs_{0.2}FA_{2.8}$ based PeLED shows a peak EQE of 18.2%, which is slightly higher than that of the $FA_{3.0}$ based PeLED (17.3%). Surprisingly, the $Cs_{0.2}FA_{2.8}$ based PeLED shows a tenfold longer lifetime than the $FA_{3.0}$ based PeLED, that is, T_{70} of 151 h and 13 h (Figure 2c), respectively, measured at a constant current density of 20 mA cm^{-2}. These observations imply that the significantly enhanced lifetime of the $Cs_{0.2}FA_{2.8}$ based PeLED benefits from a small lattice strain in the perovskite film.

2.2. Impact of the Lattice Strain on Performances of PeLEDs

To reveal the relationship between lattice strain and device performance, (Cs/FA)PbI_3 perovskite films with different amounts of Cs^+ cations are prepared, denoted as Cs_xFA_{3-x} (x represents the ratio between Cs^+ and Pb^{2+} cations in perovskite precursors). As shown in Figure S7a, Supporting Information, the XRD peaks at around 14° and 28° gradually shift to larger angles with an increasing amount of Cs^+ cations, indicating a gradual change of an FA-rich phase to a Cs-rich phase in (Cs/FA)PbI_3 perovskite films even with much excess FA^+ cations. This is further confirmed by the gradually blue-shifted absorption edges and PL peak positions (Figure S7b,c, Supporting Information) of the Cs_xFA_{3-x} perovskite films. Interestingly, as shown in **Figure 3**a, both the XRD peak positions of the (001) lattice plane and the PL peak positions show linear trends with the x value and approach the positions of pure $CsPbI_3$ perovskite[10] when x = 1.0. These observations suggest that with even much excess FA^+ cations employed in perovskite precursors, the perovskite phase of (Cs/FA)PbI_3 films are mainly determined by the amount of Cs^+ cations in perovskite precursors.

Then, we characterize the performances of PeLEDs based on Cs_xFA_{3-x} perovskite films in an x range of 0 to 0.4, in which the perovskite films show high PLQEs (Figure S7d, Supporting Information). The EL peaks (Figure 3b) of Cs_xFA_{3-x} based PeLEDs are blue-shifted with increasing x value, in line with the XRD, absorbance, and PL results of Cs_xFA_{3-x} perovskite films. As shown in Figure 3c, the statistical peak EQEs of Cs_xFA_{3-x} based PeLEDs are similar, consistent with their similarly high PLQEs. However, as shown in Figure 3d, Figures S8, and S9, Supporting Information, the lifetimes of Cs_xFA_{3-x} based PeLEDs (T_{70}, measured at a constant current density of 20 mA cm^{-2}) exhibit significant difference, which shows an inverse tendency with the $K_D\varepsilon_{rms}$ values. The PeLED based on $Cs_{0.2}FA_{2.8}$ film, which shows the minimum lattice strain, shows the longest device lifetime. The ratio of Cs^+ cation (0.2) is close to a ratio of 0.17 which is widely used in high-efficiency and stable perovskite solar cells and PeLEDs.[6a,11] These results indicate a correlation between the lattice strain and the stability of PeLEDs.

To further correlate the stability with the lattice strain, we next design another experiment. We note that other properties (e.g., crystal structure) of the Cs_xFA_{3-x} perovskite films also change with different amounts of Cs^+ cations. Therefore,

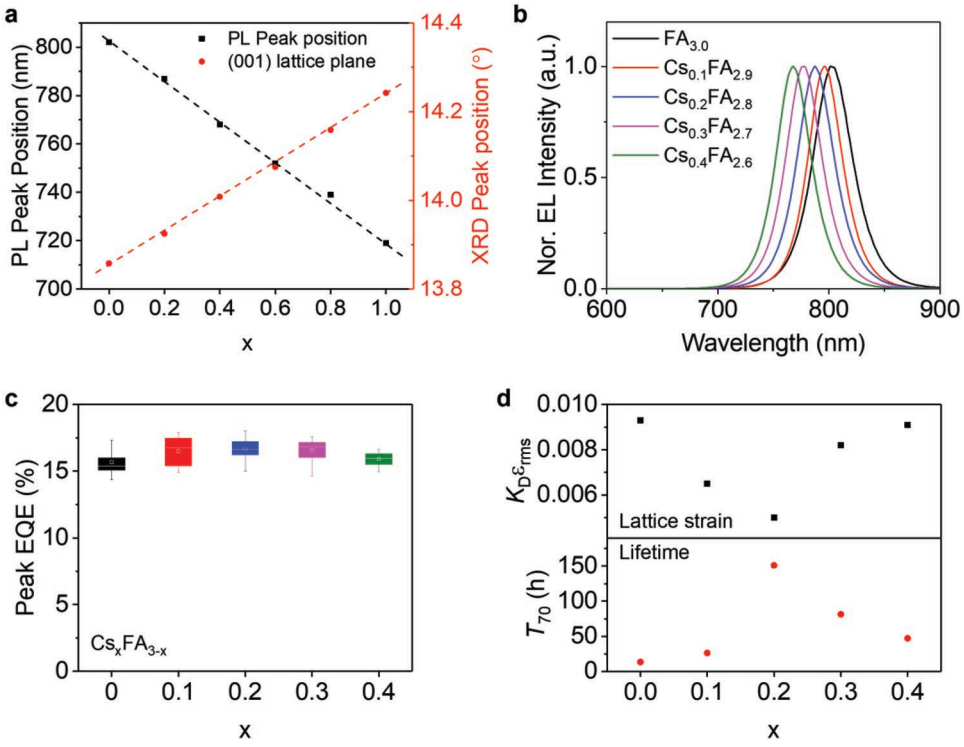

Figure 3. Properties of Cs_xFA_{3-x} perovskite films and device performances. a) PL peak and XRD peak positions of Cs_xFA_{3-x} perovskite films. b) Normalized EL spectra and c) Statistical peak EQEs of Cs_xFA_{3-x} based PeLEDs. d) $K_D\varepsilon_{rms}$ values of Cs_xFA_{3-x} perovskite films and device lifetimes (T_{70}) of Cs_xFA_{3-x} based PeLEDs.

we keep the CsI amount constant (x = 0.2, which shows the minimal lattice strain, refer to Figure 2d) and change the FAI amount in perovskite precursors. The perovskite films are denoted as $Cs_{0.2}FA_y$, where y represents the ratio between FAI and PbI_2 in perovskite precursors. For the following discussion, we focus on the y values over 2.0 (2.0, 2.4, 2.8, and 3.2), in which the (Cs/FA)PbI_3 perovskite films show the same crystal structure, absorption, and PL spectra (Figure S10 and Note S4, Supporting Information).

We first demonstrate the impact of excess FAI on the efficiency of PeLEDs. **Figure 4**a shows the PL lifetime of $Cs_{0.2}FA_y$ perovskite films, which show an increased PL lifetime with an increase of y value from 2.0 to 2.8, followed by a similar PL lifetime in the $Cs_{0.2}FA_{3.2}$ perovskite film. A similar trend is observed in the PLQEs result (Figure S11, Supporting Information). These observations indicate that excess FAI reduces trap densities of $Cs_{0.2}FA_y$ perovskite films, possibly due to a passivation role of excess FAI.[6a] As shown in Figure S12, Supporting Information, the normalized EL spectra of $Cs_{0.2}FA_y$ based PeLEDs are identical with different y values, in line with the XRD and PL results of the $Cs_{0.2}FA_y$ perovskite films. The statistical peak EQEs (Figure 4b) of the $Cs_{0.2}FA_y$-based PeLEDs improve with an increasing amount of FAI from 2.0 to 2.8, agreeing well with the PL decay and PLQE results. Hence, we conclude that excess FAI decreases the trap density of perovskite films for achieving high efficiency of PeLEDs.

Next, we correlate the lattice strain and the stability of $Cs_{0.2}FA_y$-based PeLEDs. Figure 4c and Figure S13, Supporting Information show the $K_D\varepsilon_{rms}$ values of the $Cs_{0.2}FA_y$ perovskite films. All perovskite films show similar $K_D\varepsilon_{rms}$ values around 0.0049, indicating similar lattice strain in the $Cs_{0.2}FA_y$ perovskite films with even different amounts of excess FAI. As such, excess FAI is not incorporated into the perovskite lattice and probably compensates for the FA^+ deprotonation caused by the Polyethylenimine ethoxylated (PEIE) modified ZnO nanoparticle layer (PEIE-ZnO).[12] Compared with the significant difference in the device efficiency with an increasing y value from 2 to 2.8, the lifetime of these devices is relatively constant (Figure 4d and Figure S14, Supporting Information); the slightly increased lifetime can be attributed to a better passivating result.[2b] The significant lifetime drop for the $Cs_{0.2}FA_{3.2}$ based PeLED is possibly due to exacerbated ion migration resulting from excess FAI in this device.[3b] In addition, we note that the lifetimes of PeLEDs based on $Cs_{0.2}FA_{2.0}$ (T_{70} = 95 h) and $Cs_{0.2}FA_{2.4}$ (T_{70} = 100 h) perovskite films, which exhibit minimized lattice strain, are much longer than that (T_{70} = 13 h) of the $FA_{3.0}$ based PeLED, even though they show lower EQEs than that (17.3%) of the $FA_{3.0}$ based PeLED. These results further indicate that the lattice strain is a crucial factor affecting the stability of PeLEDs.

2.3. Degradation of the Perovskite Emissive Layer

Inspired by the strong correlation between the lattice strain and the stability of PeLEDs, we investigate the degradation of the perovskite lattice structure in a long-time working condition.

We first prove that our mixed-cation (Cs/FA)PbI_3 perovskite emissive layer does not undergo phase degradation during

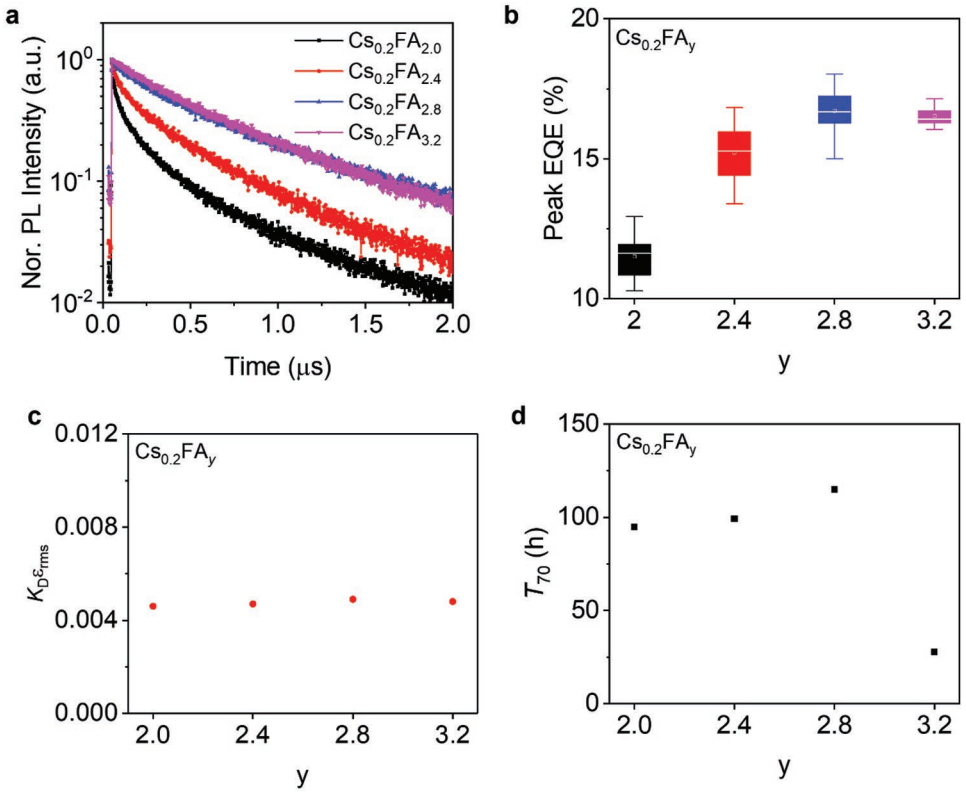

Figure 4. Characteristics of $Cs_{0.2}FA_y$ perovskite films and devices. a) PL decay curves of $Cs_{0.2}FA_y$ perovskite films. b) Statistical peak EQEs of $Cs_{0.2}FA_y$-based PeLEDs. c) $K_D\varepsilon_{rms}$ values of $Cs_{0.2}FA_y$ perovskite films. d) Device lifetimes (T_{70}) of $Cs_{0.2}FA_y$-based PeLEDs.

a long-time stability test. As shown in **Figure 5**a, working at a constant current density of 20 mA cm^{-2} for 200 h, the EL spectra of $Cs_{0.2}FA_{2.8}$ based PeLED show no peak shift, although the EL intensity continuously decreases. The first (0 h) and last (200 h) normalized EL spectra overlap with each other (Figure 5a), suggesting that our $Cs_{0.2}FA_{2.8}$ perovskites keep the same perovskite crystal structure during the testing period.[13] In addition, we perform out-of-plane 2θ XRD measurements on the same $Cs_{0.2}FA_{2.8}$ based PeLED before and after the electrical aging for 200 h. The XRD patterns of the $Cs_{0.2}FA_{2.8}$ device before and after electrical aging show the same diffraction peaks (Figure S15, Supporting Information), indicating that the $Cs_{0.2}FA_{2.8}$ perovskite film shows no decomposition after the long-time stability test. As shown in Figure 5b, the normalized XRD peaks at around 14° are also identical before and after aging, further confirming that our $Cs_{0.2}FA_{2.8}$ perovskite layer keeps the same perovskite crystal structure.

We then analyze the lattice strain of the perovskite layer before and after electrical aging. As shown in Figure 5c, the $K_D\varepsilon_{rms}$ value of the $Cs_{0.2}FA_{2.8}$ perovskite layer increases from

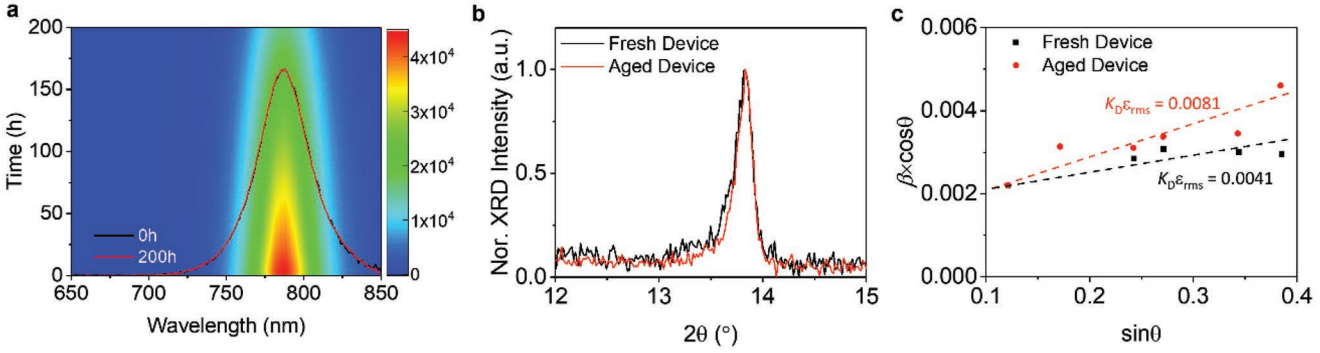

Figure 5. Degradation of $Cs_{0.2}FA_{2.8}$ based PeLED. a) EL mapping of $Cs_{0.2}FA_{2.8}$ based PeLED during stability measurement at a constant current density of 20 mA cm^{-2} for 200 h (inset: normalized EL spectra of the first and last EL spectra during the stability measurement). b) Normalized XRD patterns of (001) lattice plane and c) Williamson–Hall plots of the same $Cs_{0.2}FA_{2.8}$ based PeLED before and after electrical aging at a current density of 20 mA cm^{-2} for 200 h.

0.0041 to 0.0081 after the long-time electrical aging, indicating increased lattice strain in the $Cs_{0.2}FA_{2.8}$ perovskite layer. These results imply a change in the local perovskite lattice structure after the long-time electric aging. The situation is different in short-lived $FA_{3.0}$ PeLEDs, where the $K_D\varepsilon_{rms}$ value (Figure S16, Supporting Information) shows a slight increase from 0.0088 to 0.0095 after 20 h of electrical aging, indicating that other factors dominate the degradation in this case. Hence, we suggest that the degradation of the local perovskite lattice structure could be one of the degradation mechanisms in the long-term stable PeLEDs.

3. Conclusion

In summary, we have systematically investigated the impacts of lattice strain on the stability of high-efficiency PeLEDs based on (Cs/FA)PbI_3 perovskite films. Through the cation tailing strategy, we have demonstrated a strong correlation between the lattice strain and the stability of PeLEDs. By rationally controlling the molar ratio between Cs^+ and Pb^{2+} cations in perovskite precursors, we have achieved a minimum lattice strain in the $Cs_{0.2}FA_{2.8}$ perovskite film and a long lifetime (T_{70}) of 151 h (at a constant current density of 20 mA cm^{-2}) for the resulting high-efficiency PeLED (peak EQE of 18.2%). In addition, we have observed an increase in lattice strain after the long-time stability test, indicating that the degradation of the local perovskite lattice structure could be one of the degradation mechanisms in long-term stable PeLEDs. This work provides an insightful understanding of the relationship between lattice strain in perovskite films and device performances, as well as useful guidelines for developing PeLEDs with both high efficiencies and long lifetimes.

4. Experimental Section

Materials: Colloidal ZnO nanoparticles were synthesized following the reported solution-precipitation process.[14] Formamidinium iodide (FAI) was obtained from Dyesol. PbI_2 was obtained from TCL (≥98.0% purity). Other chemicals were obtained from Sigma-Aldrich.

Perovskite Precursor: The Cs_xFA_y perovskite precursors were prepared by dissolving CsI, FAI, PbI_2, and 4,4′-diaminodiphenyl sulfone (DDS) in N,N-dimethylformamide (DMF, anhydrous, 99.8%) solution with various molar ratios of x:y:1:1 between CsI, FAI, PbI_2, and DDS. All perovskite precursors were kept with the concentration of Pb^{2+} at 0.1 mol mL^{-1}.

Film Preparation: Indium tin oxide (ITO)-coated glasses were cleaned using an ultrasonic bath in deionized water for 15 min and then dried by high-speed nitrogen flow, followed by UV ozone for 10 min. Colloidal ZnO nanoparticles were spin-coated on the ITO substrates at 4000 rpm for 30 s in air. Then, the substrates were transported into a nitrogen-filled glovebox. Polyethylenimine ethoxylated (0.03 wt% in isopropyl alcohol) was spin-coated on the prepared ZnO substrates at 5000 rpm for 30 s, followed by thermal annealing at 100 °C for 10 min. The perovskite films were spin-coated from their precursor solutions onto the PEIE-ZnO substrates at 4000 rpm for 30 s, followed by thermal annealing at 100 °C for 5 min.

Device Fabrication: To fabricate the PeLEDs, the poly(9,9dioctylfluorene-co-N-(4-butylphenyl)diphenylamine) (TFB) in chlorobenzene (12 mg mL^{-1}) was spin-coated on the perovskite films at 3000 rpm for 30 s. Then, MoO_x (7 nm) and Au (60 nm) layers were sequentially deposited by thermal evaporation at the rates of 0.2 and 1.5 Å s^{-1}, respectively. For the single-electron devices, (2,2′,2″-(1,3,5-benzinetriyl)-tris(1-phenyl-1-H-benzimidazole) (TPBi, 35 nm), lithium fluoride (LiF, 1 nm), and aluminum (Al, 100 nm) layers were sequentially deposited on the perovskite films by thermal evaporation at the rates of 1.5, 0.1, and 5.0 Å s^{-1}, respectively.

Device Characterization: The performances of PeLEDs were measured at room temperature in a nitrogen-filled glovebox. The active device area is 0.0725 cm^2. The devices were driven with step voltages (a step of 0.05 V) for the current density-voltage curves. The current density and voltage of the devices were recorded by a Keithley 2400 source meter. The forward-viewing spectral radiant flux was measured by a homemade setup with an integrating sphere and a QE Pro spectrometer. The operational stability of the devices was measured without encapsulation in a testing box filled with nitrogen gas.[7]

Film Characterization: The perovskite films were deposited on PEIE-ZnO substrates for film characterization. Steady-state PL spectra of the films were recorded at room temperature in the air by Newton Andor with a 450 nm laser. Absorption spectra were measured with a PerkinElmer model Lambda 900. Scanning electron microscopy (SEM, Philips XL30 FEG SEM) was operated at 3 keV. STEM specimens were prepared by focused ion beam (FIB) and ultramicrotomy. STEM studies were conducted using a spherical aberration-corrected STEM (JEM-ARM200F, JEOL Co. Ltd.) equipped with a cold field emission gun and a DCOR probe Cs-corrector (CEOS GmbH) operated at 200 kV. EELS acquisition was performed by a Gatan GIF Quantum ERS imaging filter equipped with a Gatan K2 Summit camera with a convergent semi-angle of 20.4 mrad and a collection semi-angle of 111 mrad. XRD patterns were obtained from an X-ray diffractometer (Pananalytical X'Pert Pro) with an X-ray tube (Cu Kα, λ = 1.5406 Å). GIWAXS measurements were performed at BL14B1 beamline, Shanghai Synchrotron Radiation Facility (SSRF). The diffraction patterns were collected by a 2D MarCCD 225 detector at a distance of 234 mm from the samples (all the samples were protected with N_2 gas during the measurements) to the detector.

Theoretical Calculations: All first-principles calculations were based on plane-wave pseudopotential methods within density-functional theory (DFT) as implemented in the Vienna ab initio simulation package code (VASP).[15] The electrons and ions interactions were described by the projector augmented wave (PAW) pseudopotentials.[16] We used the generalized gradient approximation in the Perdew–Burke–Ernzerhof (PBE)[17] form as the exchange-correlation functional. Structural optimizations were obtained by fully relaxing all the atoms through total energy minimization with the residual forces on the atoms converged to below 0.05 eV $Å^{-1}$. The kinetic energy cut-off for the plane-wave basis was chosen to be 400 eV. To properly take into account the long-range van der Waals (vdWs) interactions that play a nonignorable role in the hybrid perovskites involving organic molecules, the Grimme's scheme (DFT+D3) method[18] was adopted. Considering the large simulation cell, we used only one k-point (gamma) to sample the Brillion zone.

Supporting Information

Supporting Information is available from the Wiley Online Library or from the author.

Acknowledgements

We thank Z. Yuan for helpful discussions. This work was supported by the ERC Starting Grant (No. 717026), the Swedish Foundation for International Cooperation in Research and Higher Education (No. CH2018-7736), and the Swedish Government Strategic Research Area in Materials Science on Functional Materials at Linköping University (Faculty Grant SFO-Mat-LiU no. 2009-00971). Z.C. is a Marie Skłodowska-Curie Fellow (No. 895679). This project has received funding from the European Union's Horizon 2020 research and innovation program under Grant Agreement No. 823717 – ESTEEM3. The authors gratefully acknowledge the support of Julia Deuschle and Birgit Bussmann during the TEM sample preparation.

Calculations were performed in part at the high performance computing center of Jilin University. The authors thank BL14B1 in SSRF for providing the beamtime. F.G. is a Wallenberg Academy Fellow.

Conflict of Interest

The authors declare no conflict of interest.

Data Availability Statement

The data that support the findings of this study are available from the corresponding author upon reasonable request.

Keywords

efficiency, lattice strain, LEDs, perovskites, stability

Received: June 28, 2022
Revised: September 5, 2022
Published online:

[1] a) X. K. Liu, W. Xu, S. Bai, Y. Jin, J. Wang, R. H. Friend, F. Gao, *Nat. Mater.* **2021**, *20*, 10; b) A. Ren, H. Wang, W. Zhang, J. Wu, Z. Wang, R. V. Penty, I. H. White, *Nat. Electron.* **2021**, *4*, 559; c) C. Bao, W. Xu, J. Yang, S. Bai, P. Teng, Y. Yang, J. Wang, N. Zhao, W. Zhang, W. Huang, F. Gao, *Nat. Electron.* **2020**, *3*, 156.

[2] a) B. Zhao, Y. Lian, L. Cui, G. Divitini, G. Kusch, E. Ruggeri, F. Auras, W. Li, D. Yang, B. Zhu, R. A. Oliver, J. L. MacManus-Driscoll, S. D. Stranks, D. Di, R. H. Friend, *Nat. Electron.* **2020**, *3*, 704; b) W. Xu, Q. Hu, S. Bai, C. Bao, Y. Miao, Z. Yuan, T. Borzda, A. J. Barker, E. Tyukalova, Z. Hu, M. Kawecki, H. Wang, Z. Yan, X. Liu, X. Shi, K. Uvdal, M. Fahlman, W. Zhang, M. Duchamp, J.-M. Liu, A. Petrozza, J. Wang, L.-M. Liu, W. Huang, F. Gao, *Nat. Photonics* **2019**, *13*, 418; c) Y.-H. Kim, S. Kim, A. Kakekhani, J. Park, J. Park, Y.-H. Lee, H. Xu, S. Nagane, R. B. Wexler, D.-H. Kim, S. H. Jo, L. Martínez-Sarti, P. Tan, A. Sadhanala, G.-S. Park, Y.-W. Kim, B. Hu, H. J. Bolink, S. Yoo, R. H. Friend, A. M. Rappe, T.-W. Lee, *Nat. Photonics* **2021**, *15*, 148; d) Y. Dong, Y. K. Wang, F. Yuan, A. Johnston, Y. Liu, D. Ma, M. J. Choi, B. Chen, M. Chekini, S. W. Baek, L. K. Sagar, J. Fan, Y. Hou, M. Wu, S. Lee, B. Sun, S. Hoogland, R. Quintero-Bermudez, H. Ebe, P. Todorovic, F. Dinic, P. Li, H. T. Kung, M. I. Saidaminov, E. Kumacheva, E. Spiecker, L. S. Liao, O. Voznyy, Z. H. Lu, E. H. Sargent, *Nat. Nanotechnol.* **2020**, *15*, 668; e) C. Sun, Y. Jiang, M. Cui, L. Qiao, J. Wei, Y. Huang, L. Zhang, T. He, S. Li, H.-Y. Hsu, C. Qin, R. Long, M. Yuan, *Nat. Commun.* **2021**, *12*, 2207; f) Z. Chu, Q. Ye, Y. Zhao, F. Ma, Z. Yin, X. Zhang, J. You, *Adv. Mater.* **2021**, *33*, 2007169; g) H. Wang, X. Gong, D. Zhao, Y.-B. Zhao, S. Wang, J. Zhang, L. Kong, B. Wei, R. Quintero-Bermudez, O. Voznyy, Y. Shang, Z. Ning, Y. Yan, E. H. Sargent, X. Yang, *Joule* **2020**, *4*, 1977.

[3] a) C. Kuang, Z. Hu, Z. Yuan, K. Wen, J. Qing, L. Kobera, S. Abbrent, J. Brus, C. Yin, H. Wang, W. Xu, J. Wang, S. Bai, F. Gao, *Joule* **2021**, *5*, 618; b) H. Wang, Z. Chen, J. Hu, H. Yu, C. Kuang, J. Qin, X. Liu, Y. Lu, M. Fahlman, L. Hou, X. K. Liu, F. Gao, *Adv. Funct. Mater.* **2020**, *31*, 2007596; c) Y. Miao, Y. Ke, N. Wang, W. Zou, M. Xu, Y. Cao, Y. Sun, R. Yang, Y. Wang, Y. Tong, W. Xu, L. Zhang, R. Li, J. Li, H. He, Y. Jin, F. Gao, W. Huang, J. Wang, *Nat. Commun.* **2019**, *10*, 3624.

[4] a) F. Ye, Q. Shan, H. Zeng, W. C. H. Choy, *ACS Energy Lett.* **2021**, *6*, 3114; b) D. Yang, B. Zhao, T. Yang, R. Lai, D. Lan, R. H. Friend, D. Di, *Adv. Funct. Mater.* **2022**, *32*, 2109495; c) Q. Dong, L. Lei, J. Mendes, F. So, *JPhys Mater.* **2020**, *3*, 012002.

[5] a) G. Kim, H. Min, K. S. Lee, D. Y. Lee, S. M. Yoon, S. I. Seok, *Science* **2020**, *370*, 108; b) M. I. Saidaminov, J. Kim, A. Jain, R. Quintero-Bermudez, H. Tan, G. Long, F. Tan, A. Johnston, Y. Zhao, O. Voznyy, E. H. Sargent, *Nat. Energy* **2018**, *3*, 648; c) Q. Cheng, B. Wang, G. Huang, Y. Li, X. Li, J. Chen, S. Yue, K. Li, H. Zhang, Y. Zhang, H. Zhou, *Angew. Chem., Int. Ed.* **2022**, *61*, 202208264.

[6] a) Y. H. Jia, S. Neutzner, Y. Zhou, M. Yang, J. M. F. Tapia, N. Li, H. Yu, J. Cao, J. P. Wang, A. Petrozza, C. P. Wong, N. Zhao, *Adv. Funct. Mater.* **2019**, *30*, 1906875; b) Y. Cao, N. Wang, H. Tian, J. Guo, Y. Wei, H. Chen, Y. Miao, W. Zou, K. Pan, Y. He, H. Cao, Y. Ke, M. Xu, Y. Wang, M. Yang, K. Du, Z. Fu, D. Kong, D. Dai, Y. Jin, G. Li, H. Li, Q. Peng, J. Wang, W. Huang, *Nature* **2018**, *562*, 249; c) K. Lin, J. Xing, L. N. Quan, F. P. G. de Arquer, X. Gong, J. Lu, L. Xie, W. Zhao, D. Zhang, C. Yan, W. Li, X. Liu, Y. Lu, J. Kirman, E. H. Sargent, Q. Xiong, Z. Wei, *Nature* **2018**, *562*, 245; d) Y. Liu, L. K. Ono, Y. Qi, *InfoMat* **2020**, *2*, 1095.

[7] H. Wang, F. U. Kosasih, H. Yu, G. Zheng, J. Zhang, G. Pozina, Y. Liu, C. Bao, Z. Hu, X. Liu, L. Kobera, S. Abbrent, J. Brus, Y. Jin, M. Fahlman, R. H. Friend, C. Ducati, X.-K. Liu, F. Gao, *Nat. Commun.* **2020**, *11*, 891.

[8] L. Q. Xie, L. Chen, Z. A. Nan, H. X. Lin, T. Wang, D. P. Zhan, J. W. Yan, B. W. Mao, Z. Q. Tian, *J. Am. Chem. Soc.* **2017**, *139*, 3320.

[9] M. L. Agiorgousis, Y. Y. Sun, H. Zeng, S. Zhang, *J. Am. Chem. Soc.* **2014**, *136*, 14570.

[10] J. A. Steele, H. Jin, I. Dovgaliuk, R. F. Berger, T. Braeckevelt, H. Yuan, C. Martin, E. Solano, K. Lejaeghere, S. M. J. Rogge, C. Notebaert, W. Vandezande, K. P. F. Janssen, B. Goderis, E. Debroye, Y.-K. Wang, Y. Dong, D. Ma, M. Saidaminov, H. Tan, Z. Lu, V. Dyadkin, D. Chernyshov, V. V. Speybroeck, E. H. Sargent, J. Hofkens, M. B. J. Roeffaers, *Science* **2019**, *16*, 679.

[11] S.-H. Turren-Cruz, A. Hagfeldt, M. Saliba, *Science* **2018**, *362*, 449.

[12] Z. Yuan, Y. Miao, Z. Hu, W. Xu, C. Kuang, K. Pan, P. Liu, J. Lai, B. Sun, J. Wang, S. Bai, F. Gao, *Nat. Commun.* **2019**, *10*, 2818.

[13] a) I. M. Pavlovetc, M. C. Brennan, S. Draguta, A. Ruth, T. Moot, J. A. Christians, K. Aleshire, S. P. Harvey, S. Toso, S. U. Nanayakkara, J. Messinger, J. M. Luther, M. Kuno, *ACS Energy Lett.* **2020**, *5*, 2802; b) Y. Lin, B. Chen, Y. Fang, J. Zhao, C. Bao, Z. Yu, Y. Deng, P. N. Rudd, Y. Yan, Y. Yuan, J. Huang, *Nat. Commun.* **2018**, *9*, 4981.

[14] J. Wang, N. Wang, Y. Jin, J. Si, Z.-K. Tan, H. Du, L. Cheng, X. Dai, S. Bai, H. He, Z. Ye, M. Lai, R. H. Friend, W. Huang, *Adv. Mater.* **2015**, *27*, 2311.

[15] a) G. Kresse, J. Furthmüller, *Comput. Mater. Sci.* **1996**, *6*, 15; b) G. Kresse, D. Joubert, *Phys. Rev. B: Condens. Matter Mater. Phys.* **1999**, *59*, 1758.

[16] P. E. Blöchl, *Phys. Rev. B: Condens. Matter Mater. Phys.* **1994**, *50*, 17953.

[17] J. P. Perdew, K. Burke, M. Ernzerhof, *Phys. Rev. Lett.* **1996**, *77*, 3865.

[18] S. Grimme, S. Ehrlich, L. Goerigk, *J. Comput. Chem.* **2011**, *32*, 1456.